TU Delft

Delft University of Technology

Bond of steel-mortar interface interfered by stray current

Chen, Zhipei; Koleva, Dessi A.; Schlangen, Erik

DOI
10.1016/j.cemconres.2021.106591

Publication date
2021

Document Version
Final published version

Published in
Cement and Concrete Research

Citation (APA)
Chen, Z., Koleva, D. A., & Schlangen, E. (2021). Bond of steel-mortar interface interfered by stray current. *Cement and Concrete Research*, *150*, Article 106591. https://doi.org/10.1016/j.cemconres.2021.106591

Important note
To cite this publication, please use the final published version (if applicable).
Please check the document version above.

Copyright
Other than for strictly personal use, it is not permitted to download, forward or distribute the text or part of it, without the consent of the author(s) and/or copyright holder(s), unless the work is under an open content license such as Creative Commons.

Takedown policy
Please contact us and provide details if you believe this document breaches copyrights.
We will remove access to the work immediately and investigate your claim.

This work is downloaded from Delft University of Technology.
For technical reasons the number of authors shown on this cover page is limited to a maximum of 10.

Green Open Access added to TU Delft Institutional Repository

'You share, we take care!' - Taverne project

https://www.openaccess.nl/en/you-share-we-take-care

Otherwise as indicated in the copyright section: the publisher is the copyright holder of this work and the author uses the Dutch legislation to make this work public.

Cement and Concrete Research 150 (2021) 106591

Contents lists available at ScienceDirect

Cement and Concrete Research

journal homepage: www.elsevier.com/locate/cemconres

Bond of steel-mortar interface interfered by stray current

Zhipei Chen [a,b,*], Dessi A. Koleva [b], Erik Schlangen [b]

[a] School of Civil Engineering, Beijing Jiaotong University, 10044 Beijing, China
[b] Microlab, Department 3MD, Faculty of Civil Engineering and Geosciences, Delft University of Technology, Stevinweg 1, 2628 CN Delft, the Netherlands

ARTICLE INFO

Keywords:
Stray current
Corrosion
Curing
Bond strength
Electrochemical properties

ABSTRACT

The focus of this work is to present test results on the bond of steel-mortar interface undergoing stray current. The bond strength, derived by pull-out tests, is correlated to the electrochemical response of the steel rebar and the properties of the mortar bulk matrix. The effects of curing regimes (in terms of duration of curing) and starting point of stray current are also investigated. It is found that stray current exerts bond degradation of the steel-mortar interface in all investigated cases, irrespective of the presence or absence of a corrodent (Cl^-) in the external medium. For the ease of operation in lab tests, the stray current is generally simulated by anodic polarization, although fundamentally, the stray current effect on the steel surface is composed of both anodic and cathodic polarizations. Hence this work also differentiates the effects of stray current on steel-mortar bond, versus the effects of anodic polarization.

1. Introduction

The bond strength of the steel-concrete interface is an important structural property for reinforced concrete structures. The stress transfer between the steel surface and the surrounding concrete via this bond "combines" the concrete and the reinforcement. The bond between ribbed bars and concrete is made up of three components: (1) chemical adhesion; (2) friction; and (3) mechanical interlocking between ribs of bars [1–3]. The bond behavior of steel-concrete/mortar interface, affected by steel corrosion, has been extensively studied in the past, where various studies report different aspects. Very few investigations, however, report on the influence of stray current on bond of steel-concrete/mortar interface.

Electric currents flow along different paths, in the earth (e.g. through soil, rock) and through conductive materials (e.g. metallic objects). Part of these currents, flowing along paths not being elements of a purpose-built electric circuit, are called stray currents [4,5]. Stray current can originate from electrified traction systems, offshore structures, marine platforms, cathodic protection systems, etc. [6]. The most frequent stray current sources are electrified traction systems (rail transits), which are also main traffic tools with accelerating urbanization all over the world. Stray currents from these systems may easily flow into the nearby structures (underground reinforced concrete structures), making stray current-induced corrosion one of the most severe forms of damage of these structures. This is because the matrix (concrete cover and soil) surrounding the steel can offer a conductive path for the stray current. Additionally, stray currents can also affect the microstructural properties of the concrete matrix [7–12].

In terms of inducing corrosion, stray direct currents (DC) are known to be much more dangerous than stray alternating currents (AC) [13–15]. The DC traction powers for railway electrification system are used in a variety of countries: 3 kV DC in Belgium and Spain, 1.5 kV DC in Netherlands, 0.75 kV DC in Southern England, etc. In this research the experimental investigations focus on stray DC.

The stray current (I_s) inducing reinforcement corrosion in a reinforced concrete element is illustrated in Fig. 1. In this case, stray current originates from the positive terminal of a foreign DC electrical source, and flows to an alternative path (underground reinforced concrete element) through the soil and concrete cover (position ① in Fig. 1). At the point ② where the stray current enters the reinforcement, a cathodic area is generated, where a cathodic reaction occurs and corresponds to a relevant cathodic polarization (ψ_c in Fig. 1). In a concrete bulk matrix (environment of high pH), the cathodic reaction is predominantly oxygen reduction, as shown in Fig. 1. The stray current would flow along the reinforcement between cathodic and anodic areas (③ in Fig. 1), where the ohmic drop (ψ_Ω in Fig. 1) would also be present. An anodic reaction (anodic polarization ψ_a, i.e., steel corrosion) will occur where the stray current flows out (is discharged) from the reinforcement (point ④). The current outflow would return to the negative terminal of the foreign DC source, "passing" through the concrete cover and soil (site ⑤), and

* Corresponding author at: School of Civil Engineering, Beijing Jiaotong University, 10044 Beijing, China
E-mail address: zhipeichen@outlook.com (Z. Chen).

https://doi.org/10.1016/j.cemconres.2021.106591
Received 14 January 2021; Received in revised form 8 August 2021; Accepted 28 August 2021
Available online 7 September 2021
0008-8846/© 2021 Elsevier Ltd. All rights reserved.

closing the electrical circuit.

Once corrosion of reinforcement starts, corrosion products form, (re) precipitate and gradually increase in volume, hence, occupy a larger volume than the parent metal. The volume expansion of corrosion products may firstly induce higher radial pressure (normal stress) between the steel surface and the concrete (mortar) cover [16,17]. This leads to an initially higher bond strength and induces splitting stress on the concrete (mortar) cover. Once the splitting stress exceeds the concrete (mortar) tensile strength, the cracks appear gradually on the concrete (mortar) cover. The ultimate consequence of corrosion is the loss of bond between the steel and the surrounding concrete.

In terms of simulating stray DC induced corrosion of metals, most references just supplied anodic polarization on samples: Ref. [9,10,18–32] applied anodic polarization for simulating stray current effects, Ref. [33–36] applied stray current. Although stray current leads to the generation of anodic locations on a steel surface, meaning that the degradation itself is linked to anodic currents and oxidation, the influence of stray current is not just anodic polarization. As presented in Fig. 1 the stray current effect is composed of both anodic polarization and cathodic polarization on steel surface. So stray current and its effects are more complex than only anodic polarization. Hence this work also differentiates the effects of stray current on bond of steel-mortar interface versus the effects of anodic polarization.

This work presents test results on the bond strength of reinforced mortar undergoing stray current and anodic polarization, conditioned in Cl-free (in water) and Cl-containing (in 5% NaCl solution) medium. The bond behavior of the steel-mortar interface, derived by pull-out tests, is correlated to the electrochemical response of the reinforcing steel and the bulk matrix properties. The effect of stray current on bond strength is discussed versus the effect of anodic polarization. The effects of the curing regimes (in terms of duration of curing) and starting point of stray currents (e.g. stray current applied at 24 h or 28 days) are also considered, by testing both 24 h (24 h)-cured and 28 days (28 d)-cured specimens of identical geometry and environmental conditions. It is found that stray current (level of 0.3 mA/cm^2) exerts bond strength degradation in all cases, irrespective of the presence or absence of a corrodent (Cl^-) in the external medium. Anodic polarization leads to more pronounced effects on the steel-mortar interface, compared to stray current, justifying that anodic polarization cannot be considered as stray current, and vice versa.

2. Experimental

2.1. Materials and specimen preparation

Stray current and anodic polarization were applied on reinforced mortar prisms (of 40 × 40 × 160 mm^3). The two cast-in Ti electrodes (MMO Ti mesh, 40 × 160 mm^2) served as terminals for anodic polarization and/or stray current application. The specimens were cast from Ordinary Portland Cement (OPC) - CEM I 42.5 N, and normed sand. The water-to-cement (W/C) ratio was 0.5; the cement-to-sand (C/S) ratio was 1:3. Construction steel (rebar) FeB500HKN (d = 6 mm), with an exposed length of 40 mm (with an exposed steel surface area of 7.54 cm^2) was centrally embedded in the mortar prisms.

The level of stray current and anodic polarization were both set at 0.3 mA/cm^2, applied as an external DC electrical field. The current density was calculated according to the exposed steel surface area. This level of current density was chosen to account for a hypothetic 10% weight loss of steel rebar, as analytically calculated via Faraday's law, for a period of 28 days in the relevant experimental conditions. Based on this calculation the level of anodic polarization corresponding to 10% mass loss over 28 d is 0.1744 mA/cm^2. Considering the fact that the supplied anodic current may be partially limited if any resistive components in the circuit would arise within the mortar bulk, the final chosen current level was increased to 0.3 mA/cm^2. The specimens' geometry and set-up for current supply were identical to those as used in Ref. [37], where alterations in the set-up relevant to this work were made to account for pull-out test (Fig. 2 and related text further below).

Prior to casting, the steel rebars were cleaned electrochemically by cathodic current of 100 A/m^2, where the steel rebar was the cathode, stainless steel was the anode. This process was performed in a solution of 75 g NaOH, 25 g Na_2SO_4, 75 g Na_2CO_3 (reagent water to make 1000 mL), according to ASTM G-1 [38]. The alignment of the bars was carefully fixed prior to the casting. The fabrication procedure of moulds and specimens is illustrated in Fig. 3. In order to produce non-contact areas between the bar and the mortar at each end of the specimen, the two ends of the bar were covered by a heat-shrinkable tube (blue parts in Fig. 2) and 60-mm-long bond breakers (i.e., PVC tubes, see Fig. 3). The heat-shrinkable tubes are aimed to avoid or minimise crevice corrosion and confine the effect of the experimental conditions to identical geometry and exposed steel surface. The de-bonding zones (bond breakers) were used to protect the reinforcement from the confining pressure of mortar at the supports, and to reduce the arching effects and end restraints [2,39] during the pull-out tests. The specimens were prepared with a relatively short embedded length (40 mm) of steel rebar, to achieve a relatively uniform bond stress distribution during the pull-out test [40,41].

2.2. Curing and conditioning

Tables 1 and 2 summarize the relevant curing and conditioning regimes, and specimens designation. After casting, all specimens were cured in a fog room (98% RH, 20 °C) for 24 h (24 h) or 28 days (28 d) until demoulding. Next, the specimens were lab-conditioned (lab air). The treatment of the specimens (after curing and demoulding) and the set-ups for current supply include 2 phases:

Phase 1 - 2/3rd of the specimens' height immersion in water or 5% NaCl for 215 days for the 24 h group (243 days for the 28 d group).

Phase 2 - Full immersion of the specimens in the same medium as Phase 1, but prolonged after 215 days onwards and until the end of the test of 490 days.

2.3. Testing methods

2.3.1. Electrochemical measurements

Electrochemical tests, including Linear Polarization Resistance

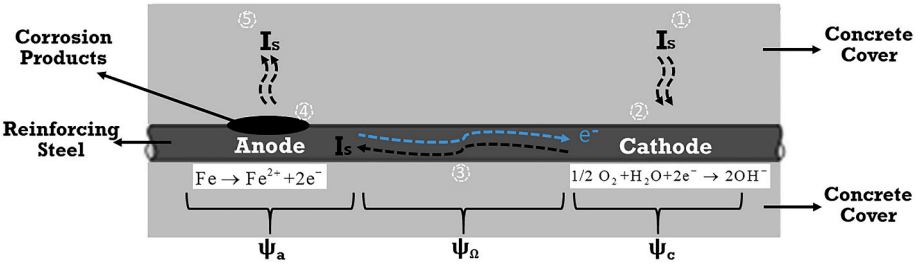

Fig. 1. Schematic of the stray current interference (I_s) on reinforcement in concrete.

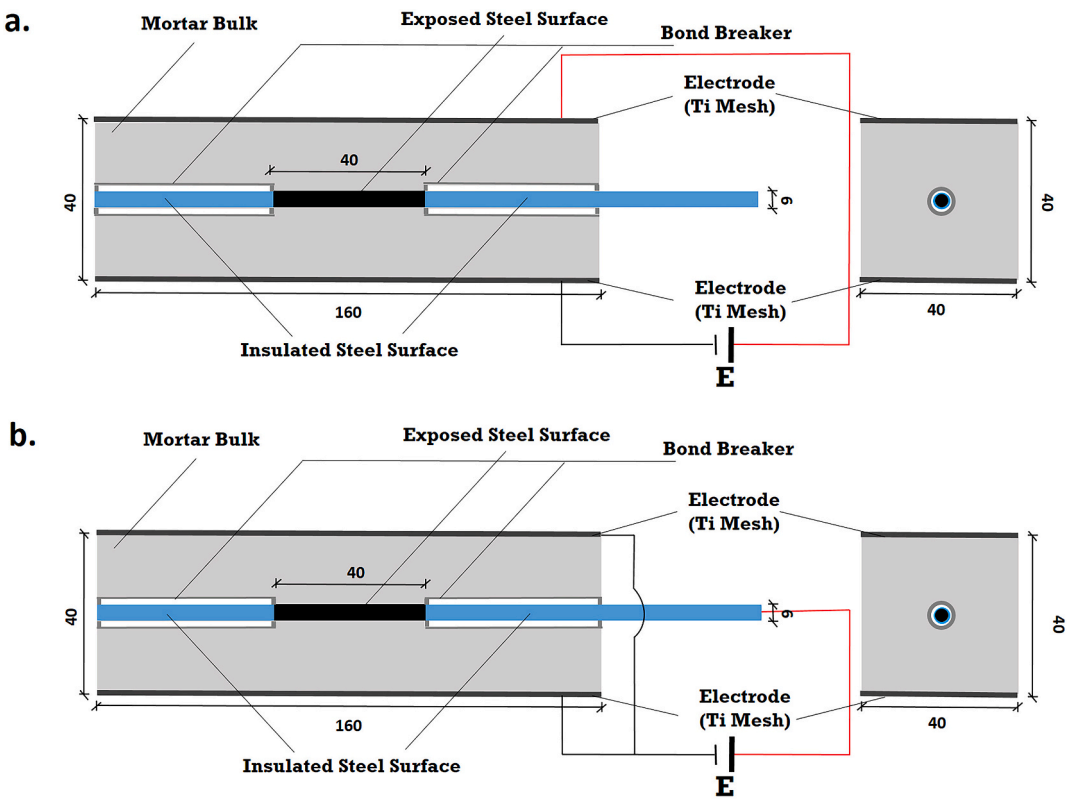

Fig. 2. Experimental set-up for current supply and position of electrodes: (a) stray current; (b) anodic polarization.

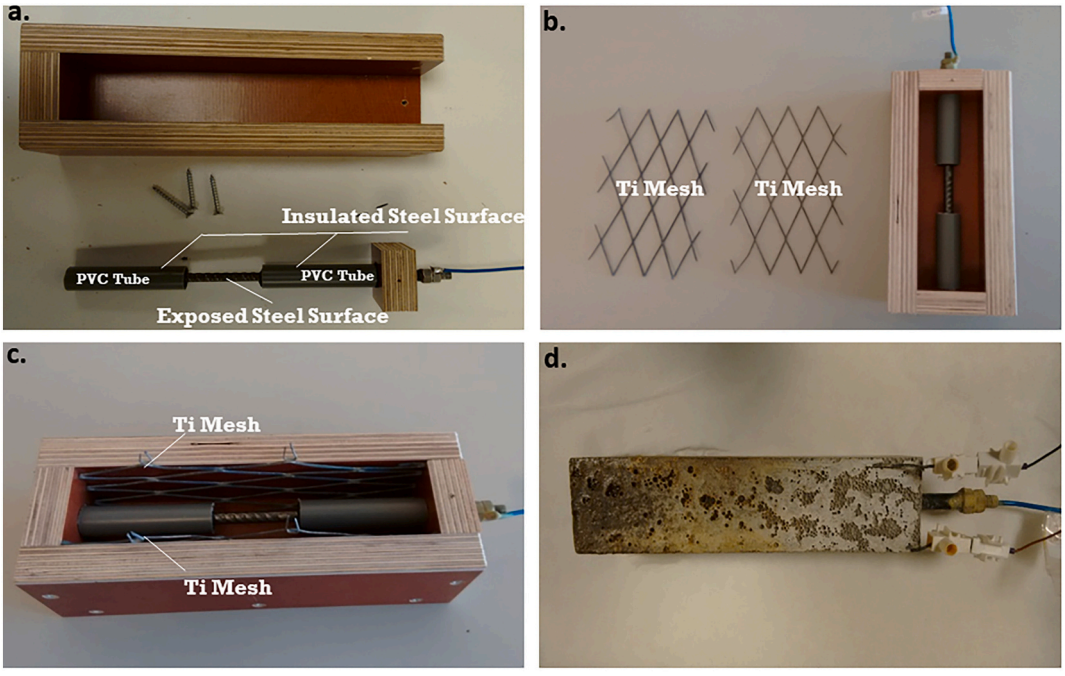

Fig. 3. Pictures of moulds and specimens fabrication.

(LPR), Electrochemical Impedance Spectroscopy (EIS) and Potentio-Dynamic Polarization (PDP) were conducted at Open Circuit Potential (OCP) for all specimens at 490 days of age. Before 243 days, to monitor the evolution of electrochemical behavior of specimens in different conditions, LPR and EIS were performed at OCP in some intervals. For the 24 h-cured specimens, both LPR and EIS tests were performed at the age of 3, 7, 14, 28, 56, 141, and 215 days. For the 28 d-cured cases, LPR and EIS tests were conducted at the age of 28 (after 1d conditioning), 35 (after 7 d conditioning), 42 (after 14 d conditioning), 56 (after 28 d conditioning), 169 (after 141 d conditioning), and 243 (after 215 d conditioning) days. In other words, the continuous/constant (at level of 0.3 mA/cm^2) stray current supply and anodic polarization were

Table 1
Summary of curing and conditioning regimes for 24 h-cured specimens[a].

Age group	0–1 d	1–215 d				215–490 d	
	Curing	Immersion (2/3rd)		Electrical field		Immersion (full)	
		Water	5% NaCl	Stray Current	Anodic Polarization	Water	5% NaCl
R-24 h	24 h	✓				✓	
C-24 h			✓				✓
S-24 h		✓		✓		✓	
CS-24 h			✓	✓			✓
A-24 h		✓			✓	✓	
CA-24 h			✓		✓		✓

[a] R-24 h: reference; C-24 h: corroding (NaCl medium); S-24 h: stray current; CS-24 h: corroding (NaCl) + stray current; A-24 h: anodic polarization; CA-24 h: corroding (NaCl) + anodic polarization – after 24 h curing.

Table 2
Summary of curing and conditioning regimes for 28 d-cured specimens[a].

Age group	0–28 d	28–243 d				243–490 d	
	Curing	Immersion (2/3rd)		Electrical field		Immersion (full)	
		Water	5% NaCl	Stray current	Anodic polarization	Water	5% NaCl
R-28 d	28 d	✓				✓	
C-28 d			✓				✓
S-28 d		✓		✓		✓	
CS-28 d			✓	✓			✓
A-28 d		✓			✓	✓	
CA-28 d			✓		✓		✓

[a] R-28 d: reference; C-28 d: corroding (NaCl medium); S-28 d: stray current; CS-28 d: corroding (NaCl) + stray current; A-28 d: anodic polarization; CA-28 d: corroding (NaCl) + anodic polarization – after 28 d curing.

interrupted at these ages. For specimens undergoing stray current or anodic polarization, a 24-hour de-polarization (potential decay) was performed prior to any further testing. The experimental protocol and the sequence of tests can be seen in [37]. The evolutions of LPR and EIS before 243 days were reported in [37]. Prior to and during the electrochemical tests the specimens were immersed fully in the relevant aqueous medium. The two Ti electrodes (connected with each other) served as counter electrode in a general 3-electrode set-up, where the rebar was the working electrode and an external Saturated Calomel Electrode (SCE) served as a reference electrode.

Linear Polarization Resistance (LPR) was performed in the range of ±20 mV (vs OCP), at a scan rate of 0.1 mV/s. This method allows determination of polarization resistance (R_p). The R_p values are used for a quantitative assessment, through calculating corrosion current by employing the Stern-Geary equation, i.e., $i_{corr} = B/R_p$ [42]. The R_p value was experimentally derived, whereas for the constant B the reported values for passive (B = 52 mV/dec) or active (B = 26 mV/dec) were employed [43,44]. Since R_p is inversely proportional to the corrosion current, quantification of corrosion resistance can be performed by a comparative analysis of R_p values only, as used and discussed in this work.

In order to account for a more accurate assessment of the bulk matrix characteristics, the EIS tests here were conducted in the maximum frequency range that can be supported by the instrument, by superimposing an AC voltage of 10 mV (rms). In this work EIS was performed in the full frequency range of 1 MHz to 10 mHz, to offer information for both the property of the bulk matrix (high to middle frequency - HF to MF range of EIS) and the electrochemical response of the embedded steel (low frequency - LF range of EIS).

In order to collect additional information of the electrochemical state of the steel surface, PDP was finally performed in the range of −0.15 V to +0.90 V (vs OCP) at a scan rate of 0.5 mV/s. The properties of both bulk matrix and steel surface obtained by electrochemical measurements will be correlated to the bond behavior. The used equipment for electrochemical tests in this work was Metrohm Autolab (Potentiostat PGSTAT302N), combined with a FRA2 module.

2.3.2. Pull-out test

After the electrochemical tests, pull-out tests were performed on all specimens. The pull-out test set-up followed the specification of ASTM C-234-91a [45] and was performed with a stiff test frame (647 Hydraulic Wedge Grip, MTS Systems Corporation) at loading rate of 0.01 mm/s under displacement control. A steel frame connected to the testing machine was designed and fabricated, to accommodate the specimens on the top of a bearing plate. The test machine and setup for pull-out tests are illustrated in Fig. 4.

The load-slip curve (relationship) was recorded. The applied load (F) was measured with the help of a force sensor, whose signal was fed to an automatic data acquisition system. The loaded-end slip was measured with the help of 2 LVDTs, output of which is an average value of these 2 LVDTs. Bond stress (τ) was obtained according to: $\tau = F/\pi dl$ (d = 6 mm of diameter of rebar, l = 40 mm of exposed length of rebar, F = recorded pull-out force), i.e., the pull-out force was divided by the corresponding embedded area of steel to obtain the bond stress.

3. Results and discussion

3.1. OCP and R_p

The OCP and R_p values recorded via LPR measurements at the conditioning stage of 490 days are depicted in Fig. 5a for Cl-free specimens, and in Fig. 5b for Cl-containing cases. The impact of curing on the electrochemical properties of steel embedded in the mortar specimens, is evident from the recorded differences in OCP and R_p values between specimens designated 24 h and those with 28 d designation. For instance, as expected the R-28 d specimens show more noble OCP values (around −240 mV vs SCE) and higher R_p (ca. 230 kΩ/cm^2) than R-24 h (Fig. 5a), reflecting the higher corrosion resistance of R-28 d. This implies the importance of sufficient curing on passive layer formation, for reinforcing steel embedded in mortar. Anodic polarization, also as expected, induces the formation of corrosion products on the steel surface (anodic polarization leads to steel dissolution). Hence, an enhanced corrosion state of the steel surface is relevant for specimens with designation "A", compared to those in stray current conditions for both 24 h-cured and 28 d-cured situations: the R_p of A-24 h/A-28 d are lower than those of S-24 h/S-28 d. This is especially the case for the 28 d-cured group, where a significantly lower R_p is recorded for specimen A-28 d if compared to specimens S-28 d (Fig. 5a).

If a comparison is made between R-24 h (control, cured for 24 h) and S-24 h (cured for 24 h + stray current), a more active state is related to S-24 h (a more cathodic OCP and a lower R_p than R-24 h). However this is not observed for the 28 d-cured cases, where similar R_p values for S-28 d and R-28 d are recorded at the age of 490d. This means that the stray current effect in sufficiently cured specimens is not as obvious as this would be in a non-mature matrix, as for instance in the case of the only 24 h-cured cases (Fig. 5a). In Cl-free (conditioned in water) situation,

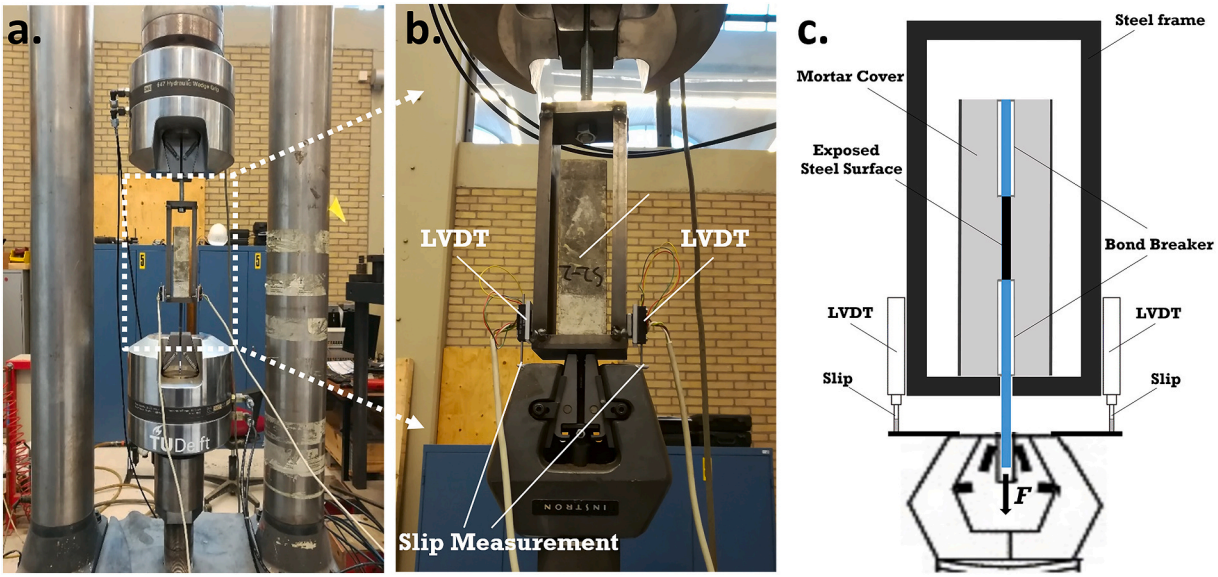

Fig. 4. Pull-out measurement setup.

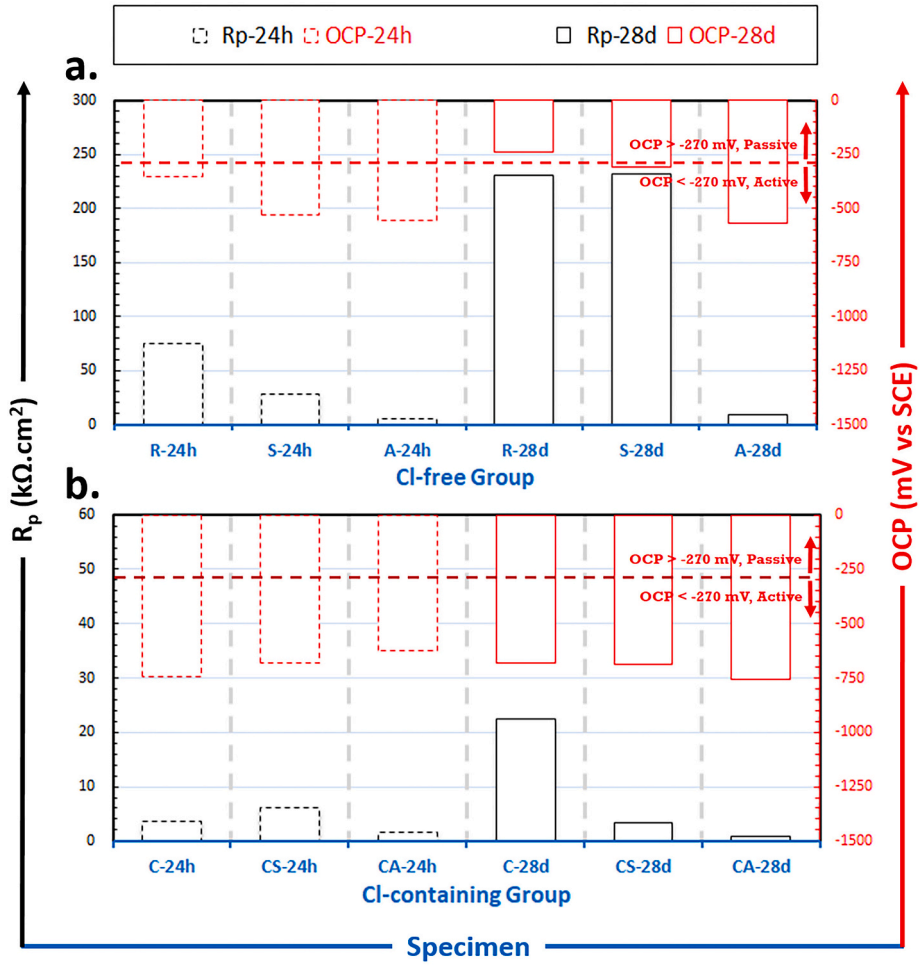

Fig. 5. OCP and R_p values (derived from LPR) of specimens at 490 days. (a) Conditioned in water; (b) conditioned in 5% NaCl.

stray current flowing through the fresh (non-mature) bulk matrix, may lead to enhanced migration of water and ions. In this case the cement hydration and steel surface passivation can be enhanced [7,46,47]. However, this phenomenon is not evident for the condition of sufficiently cured bulk matrix, as the bulk matrix is already hardened when the stray current is supplied.

At age of 490 days, the OCP and R_p values of A-24 h and A-28 are in the same range. This means that the electrochemical state of the steel

surface in A-24 h and A-28 d specimens is similar at the end of conditioning. However, macro-cracks are observed on the mortar cover of A-24 h, but such are not found for A-28 d.

The OCP values for the Cl-containing specimens remain at very negative (cathodic) levels (see Fig. 5b, in the range between −620 mV and −760 mV, vs SCE). This, together with the recorded low R_p values, reflects the accelerated corrosion state of the steel rebar affected by Cl^-. For the C-24 h and C-28 d, higher OCP and R_p are observed for C-28 d, showing the more active state of the former, C-24 h case, and the highest corrosion resistance among all "C" cases in the latter, C-28 d case. This indicates again the significance of sufficient curing/hydration of bulk matrix.

For cases CS-24 h and CS-28 d (stray current + Cl^-), CS-24 h is more corrosion resistant compared to CS-28 d (more anodic OCP and higher R_p of CS-24 h, than CS-28 d). This is related to the application of stray current at very early age (24 h) for the group of specimens CS-24 h. At this very early age the stray current played roles in affecting both "fresh" bulk matrix and the steel surface. As previously reported, the stray current has positive effects on "fresh" bulk matrix because of accelerated hydration, induced by ion migration and water transport at early age. In contrast, ion and water transport due to migration are relatively impeded in CS-28 d specimens, where the stray current was supplied at the age of 28 days and, the mortar bulk was already hardened. In this case the positive effect of stray current on the bulk matrix is not significant. This is because of the lower porosity and lower pore interconnectivity in CS-28 d, hence, impeded stray current flow.

CA-24 h and CA-28 d (NaCl + anodic polarization) show a much more severe corrosion state than CS-24 h and CS-28 d (NaCl + stray current), which is well supported by the recorded significantly lower R_p values of CA-24 h and CA-28 d. In Cl-containing specimens, anodic polarization does not only dissolve the steel, but also accelerates Cl^- ion migration towards the steel-mortar interface.

The OCP and R_p values derived from LPR only provide global corrosion resistance, but cannot reflect the charge transfer processes, product layer properties and transformations, which are related to the steel surface characteristics and bond property. Hence, more detailed information of steel surface properties under different conditions will be further discussed based on the observations of PDP and EIS response in Sections 3.3 and 3.4, together with the correlation of electrochemical response and bond behavior, as derived from pull-out test. The pull-out test results will be shown and discussed in next Section 3.2.

3.2. Pull-out test results

Fig. 6 depicts the bond stress-slip relationships for all specimens. A comparison of the bond strength (as reflected by the peak of the pull-out curves in Fig. 6) for all specimens can be seen in Fig. 7. It can be noted that stray current leads to bond degradation of the steel-mortar interface, regardless of the presence or absence of Cl^- in the external environment. The actual specimens after pull-out are shown in Figs. 8–12

For the 24 h-cured Cl-free cases (Fig. 6a), the maximum bond strength (19.6 MPa) is observed for the control specimen (R-24 h). The sharp drop of bond stress after the peak occurs earlier for S-24 h, corresponding to a 9.1% reduction of bond strength for S-24 h, 17.8 MPa, compared to R-24 h. A remarkable decrease (60.6%) of bond strength (7.7 MPa) is found for A-24 h. The bond stress of A-24 h is abruptly lost by the split of mortar along the steel rebar. The induced longitudinal cracks can be seen in Fig. 9.

As can be seen in Fig. 6b, the reduction of bond strength is observed for S-28 d compared to R-28 d (12.7% decrease, from 19.9 to 17.3 MPa).

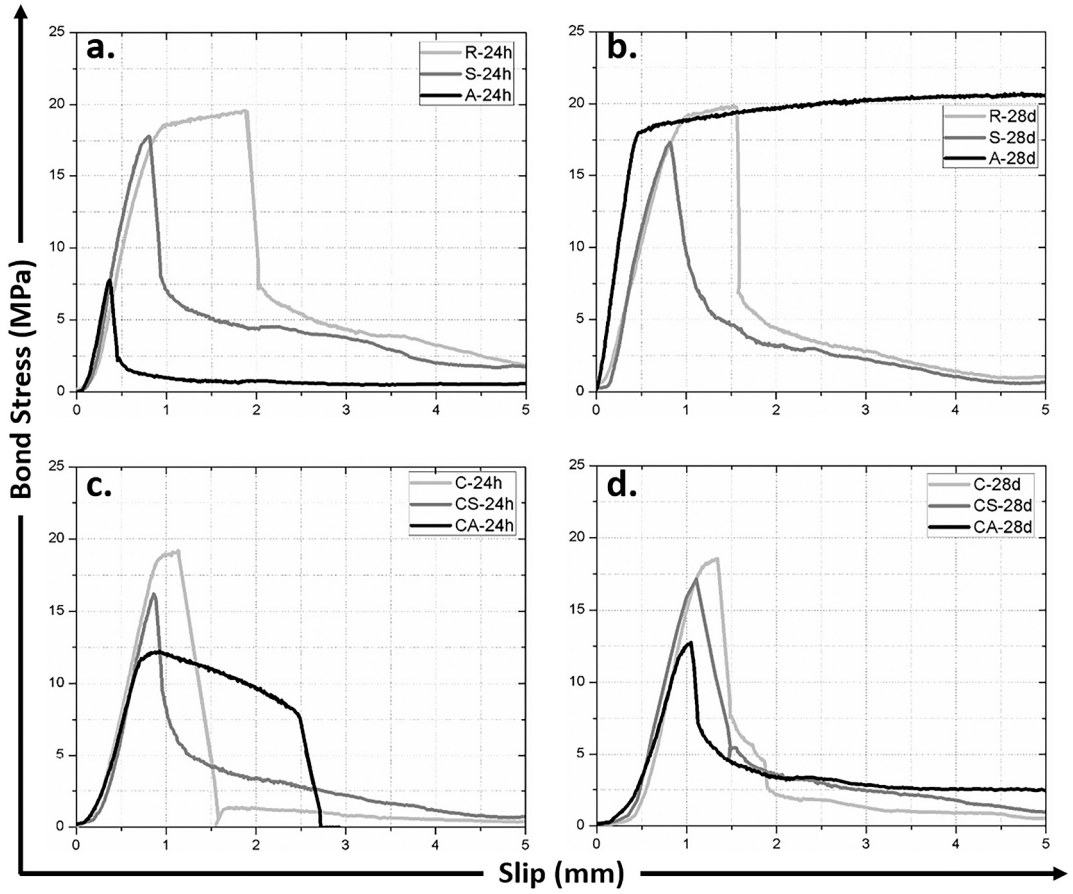

Fig. 6. Bond stress-slip relationship of: (a) 24 h-cured specimens treated in water; (b) 28 d-cured specimens treated in water; (c) 24 h-cured specimens treated in 5% NaCl; (d) 28 d-cured specimens (treated in 5% NaCl).

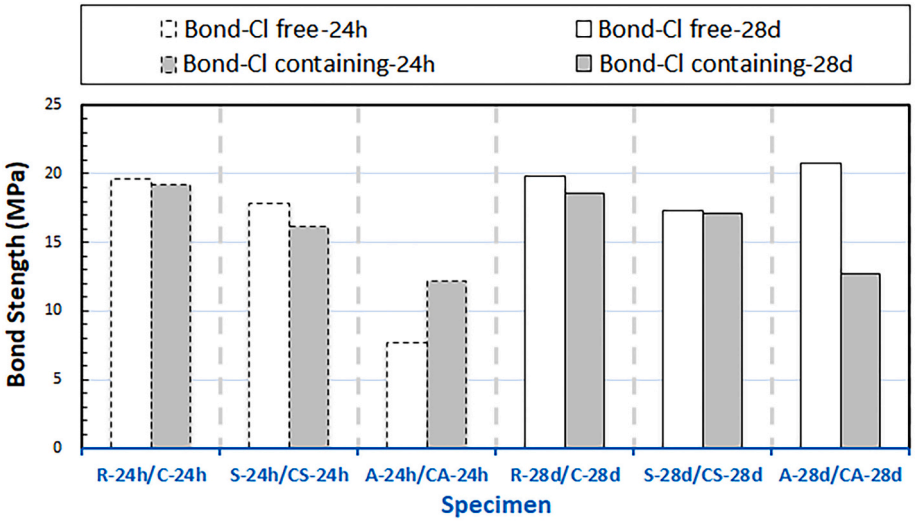

Fig. 7. Comparison of bond strength of all specimens.

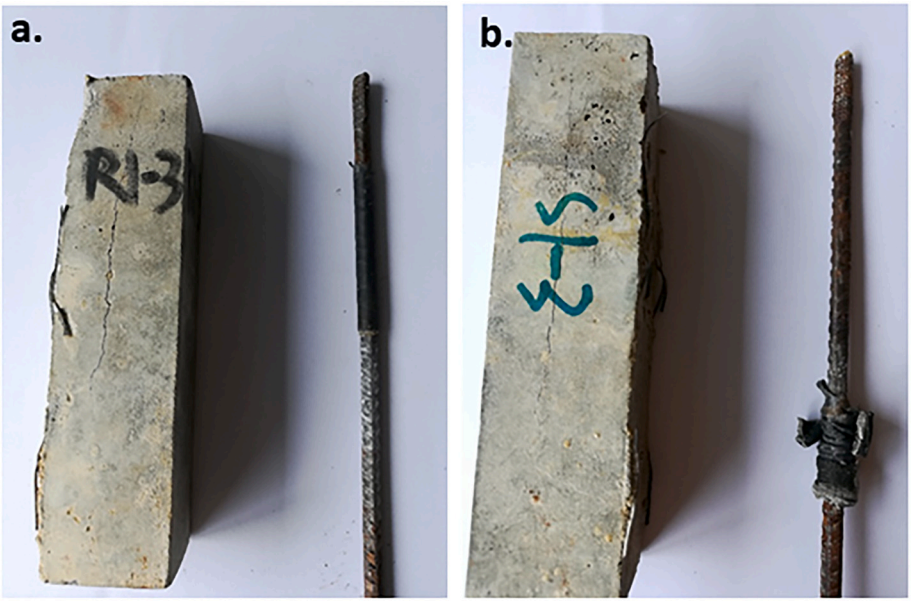

Fig. 8. Specimens after pull-out: (a) R-24 h; (b) S-24 h.

Similar to the 24 h-cured situation, a premature drop of bond stress occurs for S-28 d. For A-28 d, although a pronounced reduction in corrosion resistance is recorded (as shown in Fig. 5a, low R_p and cathodic OCP value of A-28 d), a bond loss for A-28 d specimen is not found. As shown in Fig. 10c, the failure mode of A-28 d is yielding/rupture of the rebar. This means that the bond capacity of this steel-mortar interface is higher than the tensile strength of the rebar (higher than 20.8 MPa). The high bond strength is attributed to the increase in normal stress at steel-mortar interface, caused by the formation and expansion of corrosion product at the steel-mortar interface. To be noted here is also the fact, that for a relatively mature matrix, as the case of A-28 d, the initial corrosion products confinement would be more significant if compared to A-24 h (presented in Fig. 7). For the 24 h-cured specimen A-24 h, a more open and porous matrix would determine formation, accumulation, dissolution and re-precipitation of corrosion products within the bulk matrix overall, rather than confinement at the steel-mortar interface, as in A-28 d. For A-28 d a visible crack is not induced, although the expansion of corrosion product develops mechanical pressure on the surrounding mortar. In contrast, for A-24 h, macro-cracks are observed, together with a reduced bond strength. More details related to this will be discussed together with PDP and EIS, in the next sections.

For the effects of Cl^- induced corrosion on bond: compare C-24 h to R-24 h (C-28 d to R-28 d), a decreased bond strength is recorded for the Cl-containing specimens, as shown in Fig. 7. For CS-24 and CS-28 d (stray current + Cl^- specimens), a decrease of bond strength induced by stray current can again be observed in both 24 h and 28 d-cured situations, i.e., reduction of 15.5% (from 19.2 MPa to 16.2 MPa) for C-24 h and CS-24 h, 7.7% (from 18.6 MPa to 17.1 MPa) for C-28 d and CS-28 d. The most remarkable bond loss is related to the "Cl^- + anodic polarization" cases. For CA-24 h, a rupture of the steel bar is observed, as shown in Fig. 11. This is because of the reduced cross-section of steel for CA-24 h. A significantly low bond strength (only 12.7 MPa) is recorded for CA-28 d. After pull-out, loss of cross-section of the steel rebar is observed on specimen CA-28 d, as shown in Fig. 12c.

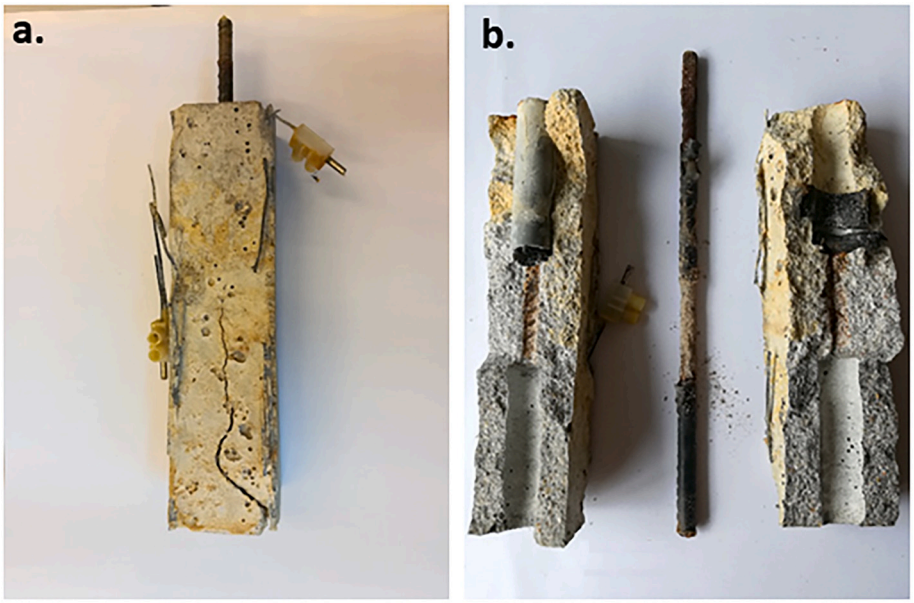

Fig. 9. Specimen A-24 h: (a) before pull-out; (b) after pull-out.

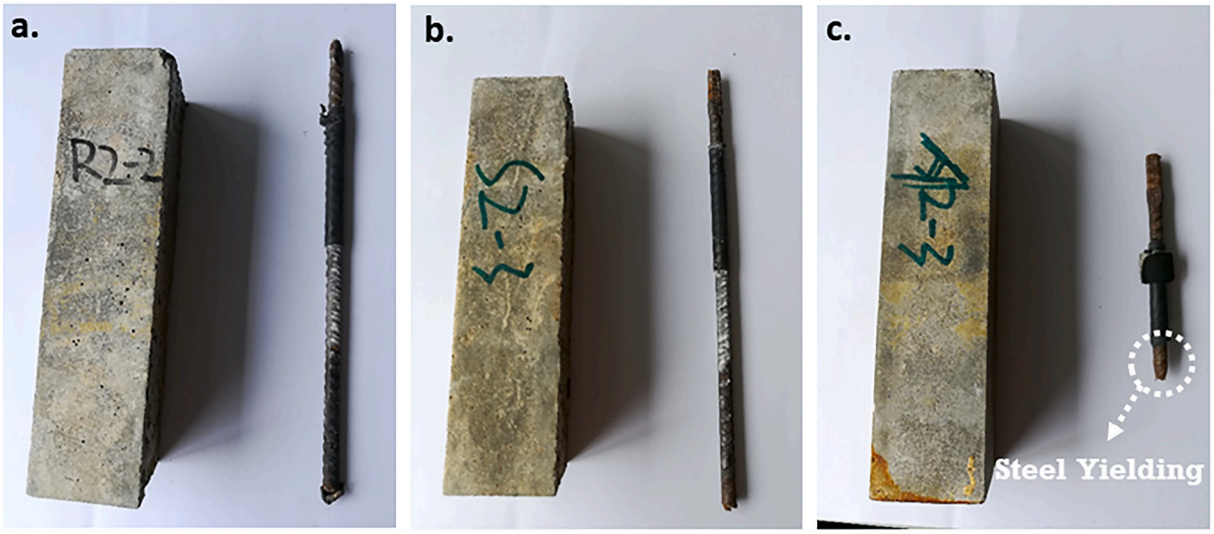

Fig. 10. Specimens after pull-out: (a) R-28 d; (b) S-28 d; (c) A-28 d.

3.3. PDP

3.3.1. PDP response of Cl-free specimens

PDP curves of all specimens are presented in Fig. 13. For these Cl-free cases (Fig. 13a), the most noble corrosion potential (approx. −220 mV) and lowest corrosion current are recorded for the specimen R-28 d (the control specimen cured for 28 d) - as expected and in line with the OCP and LPR results in Fig. 5a. In accordance with the much lower R_p values derived from LPR, high anodic current and cathodic corrosion potential (approx. −550 mV) are recorded for A-24 h and A-28 d.

It can also be noted that limitations within the anodic polarization are observed for A-28 d (although the anodic currents remain high if compared to those of specimens R-28 d and S-28 d, Fig. 13a). Additionally an anodic peak around −210 mV (vs SCE) is observed for the case of A-28 d (with current density peak of 11.43 μA/cm^2). This is related to the dissolution of iron oxide/hydroxide layer previously formed on the steel surface.

Both of above observations mean that a relatively stable and compact product layer exist on the steel surface of A-28 d, and cause limitations to the dissolution process within anodic polarization. In an alkaline environment the main corrosion product of iron is $Fe(OH)_2$ [48]. By anodic polarization of iron, Fe(III) may be formed directly on the electrode surface as Fe_2O_3, as mixed iron oxide (including Fe_3O_4) or as FeOOH [49,50]. These corrosion products have higher volume than the original steel itself, and occupy a greater volume at the steel-mortar interface. Since the bulk matrix of A-28 d is sufficiently cured, hence a less porous matrix (with less water) is present at steel-mortar interface. This means that the corrosion product cannot easily penetrate into the surrounding bulk matrix, and a more confined product layer is at hand, which is also reflected by the anodic limitation of PDP response. In this situation the corrosion product growth, dissolution and (re)precipitation are restricted (the mortar cover is sufficiently cured and hardened, cracks are not induced for A-28 d at the end of conditioning). This further leads to the compacted product layer and limitations to a steel dissolution process. This supports the bond behavior derived from the pull-out test (Fig. 6b): the highest bond strength is recorded for A-28 d.

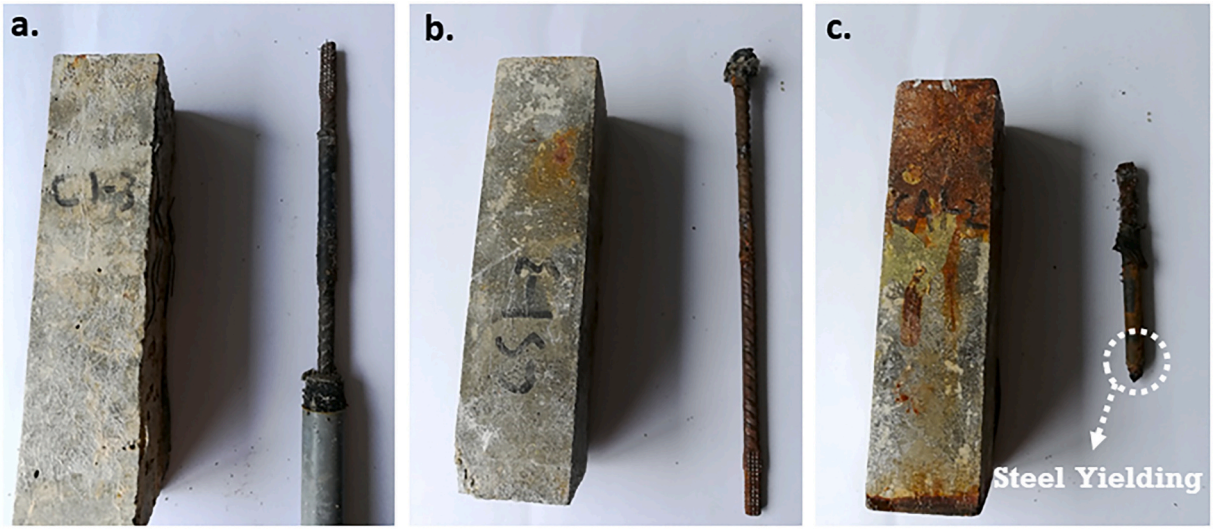

Fig. 11. Specimens after pull-out: (a) C-24 h; (b) CS-24 h; (c) CA-24 h.

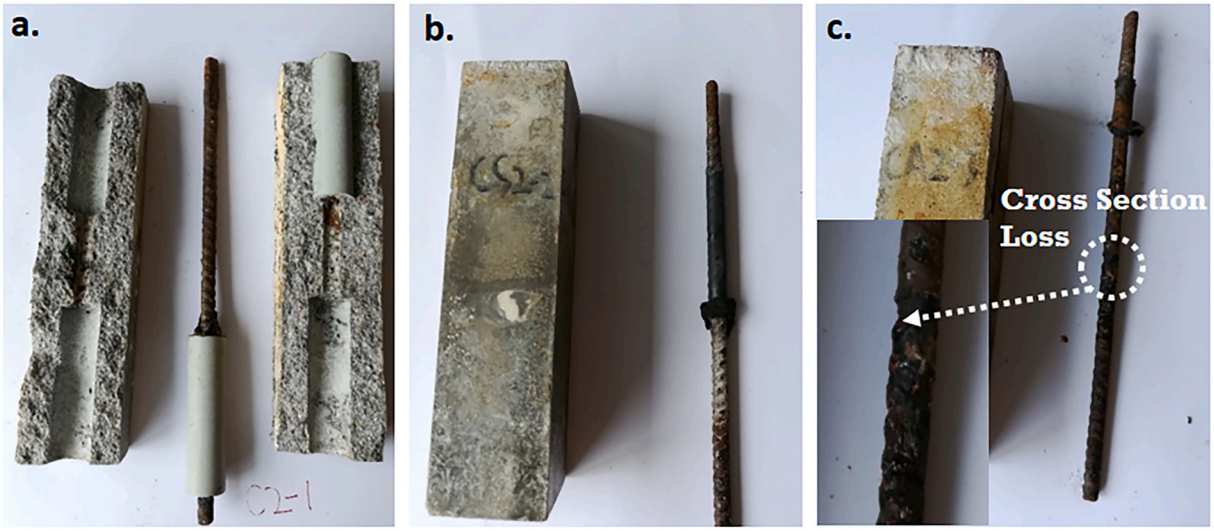

Fig. 12. Specimens after pull-out: (a) C-28 d; (b) CS-28 d; (c) CA-28 d.

For specimen A-24 h (Fig. 13a), anodic currents limitation after ca. −210 mV are not pronounced (for A-24 h only 24 h curing was relevant, after which anodic polarization was applied). The anodic current of A-24 h is almost one order higher than that of A-28 d. The PDP response of A-24 h reflects a presumably unstable and porous corrosion product layer. This is attributed to the crack induced by the continuous product layer growth starting at very early age. For A-24 h, at early age the bulk matrix surrounding steel surface is porous (also with a higher water content, compared to A-28 d). In this situation the corrosion products disperse into the matrix more easily. In other words, the corrosion product layer is more porous and less homogeneous (i.e., compromised ITZ properties), compared to A-28 d. Additionally, the mortar cover was cured in fog room for only 24 h (i.e., not cured sufficiently, not fully hydrated), the strength of mortar is also lower than that of A-28 d. The consequence of this is crack propagation. Once macro-cracks are induced, the environmental condition in the vicinity of steel surface will be changed (H_2O and oxygen penetrate to the vicinity of the steel surface via cracks). This will allow an ongoing process of corrosion product formation, (re)precipitation and transport towards voids and cracks in the bulk matrix. The ultimate consequence is the loss of steel-mortar bond (reduced bond strength of A-24 h is recorded in Fig. 6a). These properties and behavior can also be reflected by the EIS response, and will be further discussed in the next section.

For the 24 h-cured control specimen (R-24 h), a more active state (compared to R-28 d specimen) is recorded (more cathodic potential and higher anodic current than R-28 d). The recorded corrosion current of S-24 h (cured for 24 h, followed by supply of stray current) is one order higher than that of specimen R-24 h, accompanied by a more cathodic potential (about −520 mV). Different from R-24 h, anodic limitation is observed after the OCP for S-24 h. After this, the first current density peak of 5.16 $\mu A/cm^2$ is observed at around −210 mV (vs SCE), and the second current density peak of 10 $\mu A/cm^2$ is observed at around 10 mV (vs SCE). These peaks are related to the dissolution of $Fe_2O_3{\cdot}nH_2O$ and/or a mixture of oxide and hydroxide [51,52].

These phenomena (the peaks and anodic limitation after corrosion potential) however are not significant for S-28 d, reflecting that in the case of S-24 h specimen, a product layer of different composition and/or distribution on the steel surface was formed. This is also in accordance with the pull-out result: the bond strength of S-24 h is higher than S-28 d (Fig. 7), although higher anodic current density is recorded for S-24 h (see the PDP response in Fig. 13a). This recorded difference between S-24 h and S-28 d is again related to the curing regimes, and illustrates the

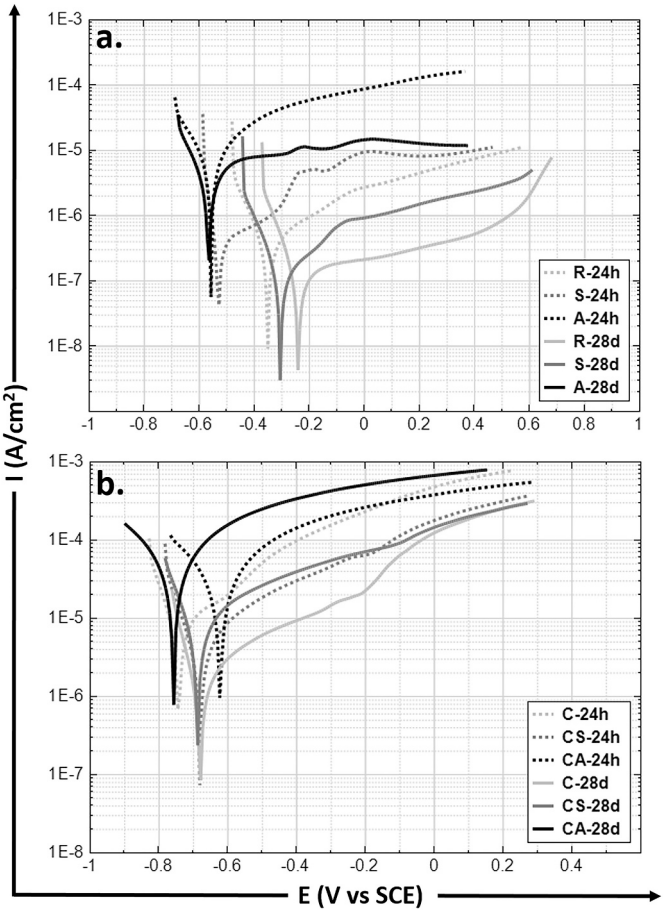

Fig. 13. Overlay of PDP curves for specimens at 490 days: (a) specimens in water; (b) specimens in 5% NaCl.

importance of the starting time of stray current supply: at very early age (24 h in present work), the stray current induced a more significant interference than the case of later age (after 28 days).

3.3.2. PDP response of Cl-containing specimens

As can be observed in Fig. 13b, a cathodic corrosion potential is evident for the Cl-containing specimens (more cathodic than −600 mV). Additionally, the corrosion current densities for these specimens are significantly higher, compared to the cases treated in water. The most pronounced corroding state is related to specimens, subjected to both anodic polarization and Cl-containing medium (CA-24 h and CA-28 d). If a comparison is made between specimens C-24 h and CS-24 h, the pronounced effect of the stray current in group CS-24 h towards enhanced corrosion is not observed: the corrosion current density of CS-24 h is even lower than that of specimens C-24 h. This relatively higher corrosion resistance in specimen CS-24 h reflects the potentially positive effect of the stray current at very early age, because of enhanced cement hydration. This will result in a faster development of pore network, and lead to a more rapid stabilization of the pore solution and hydration products.

Based on this, competitive mechanisms would be relevant for specimen CS-24 h. On one hand, the stray current has positive effects on the bulk matrix properties at early age (in a fresh matrix). On the other hand stray current accelerates Cl^- ion migration, and enhances steel corrosion, finally results in a corrosion products build-up on the steel surface. The recorded lower bond strength of CS-24 h (compared to C-24 h, where only Cl-induced corrosion plays a role) is in line with this. Again, the different electrochemical state of CS-24 h, compared to C-24 h, can be reflected by the EIS, and will be discussed later on in Section 3.4.3.

In contrast to the above sketched different performance of C-24 h and CS-24 h, this difference is not obvious in the 28 d-cured specimens (C-28 d and CS-28 d). It can be observed via PDP (Fig. 13b) that the steel surface of CS-28 d shows more corrosion than C-28 d. In other words, the stray current effect for 28 d-cured specimen leads to accelerated steel corrosion. For CS-24 h, at the age of 1–28 days, the stray current already played roles (positive and negative) in both affecting the "fresh" bulk matrix and the steel surface. For the 28 d-cured specimen CS-28 d, the stray current exerts mainly negative effects, predominantly affects the steel.

According to the PDP responses, it is clear that anodic polarization (A or CA groups) leads to a more active status of the steel surface than stray current (S or CS groups), in all conditions investigated in the present work. The different effects of stray current and anodic polarization on bond of steel-mortar interface will be further discussed, together with EIS response in the next section.

3.4. EIS

3.4.1. General consideration for EIS fitting

The EIS experimental results for all investigated specimens are shown in Figs. 14 and 15, in Nyquist formats. All impedance plots present values in Ω, since the geometries of the cells and the steel surface are identical. The equivalent electrical circuit used for fitting the EIS response can be seen in Fig. 16a: R_0 represents the electrolyte resistance; R_1 is the resistance of the solid phase of mortar cover, the capacitance C_1 represents the dielectric capacitance of solid phase of mortar cover; C_2 and R_2 are related to double layer effects and ionic motion in pore network; R_3 and Q_3 are related to the bulk matrix in the vicinity of steel-mortar interface; $R_4(R_p)$ and Q_4 correspond to the charge/mass transfer processes, linked to the electrochemical reaction on the steel surface [53–55], i.e., the R_{ct} and $R_{red/ox}$ make up R_p. For deriving R_p from EIS measurements in reinforced concrete/mortar, the low frequency limit of the impedance spectra is generally considered for calculations, as reported in Ref. [56–60] and used in the present study as well. The replacement of pure capacitance (C) with constant phase element (CPE or Q) in the equivalent circuits is widely accepted for systems as in this study, denoted to in-homogeneities at different levels, hereby being mainly relevant to the heterogeneity of hydration/corrosion products, that form on the steel surface in different conditions [58,61–64].

The EIS fitting process was performed by NOVA software package (Version 1.11). An example (EIS response of S-28 d at age of 490 days) for the experimental response and fit of the studied specimens in this work is presented in Fig. 16b in both Nyquist and Bode format. It can be seen that the proposed circuit - [R(CR[CR])(Q[R(QR)])], Fig. 16a, involves elements with a clear physical meaning and gives generally good fitting results. The obtained parameters were considered mainly for comparative purposes (derived via identical electrical circuit, fitting procedure and error plots with a x^2 in the order of 0.01), rather than as absolute values.

Although a clear comparison of the bulk matrix properties, including the steel-mortar interface (HF response), and the electrochemical state of the steel reinforcement (LF response) is possible by only qualitative assessment of the EIS responses in Figs. 14 and 15, quantification of the cases of interest only is also presented and discussed in view of main parameters as bulk matrix resistance (R_{bulk}) and polarization resistance (R_p). The interest here is to clarify the different effects of stray current and anodic polarization, in perspective of bond strength of steel-mortar interface; and to correlate the bond behavior of steel-mortar interface with the electrochemical response of reinforced mortar specimens, affected by stray current and anodic polarization. Hence in order to illustrate the above points, the results from EIS fitting for groups S-24 h, A-24 h, S-28 d and A-28 d (cases only related to stray current and anodic polarization) are shown in Figs. 17 and 18 as EIS-derived parameters for mortar bulk properties (R_{bulk}) and steel corrosion resistance (R_p).

As can be seen in Figs. 14 and 15, the HF domain (higher than 1 kHz)

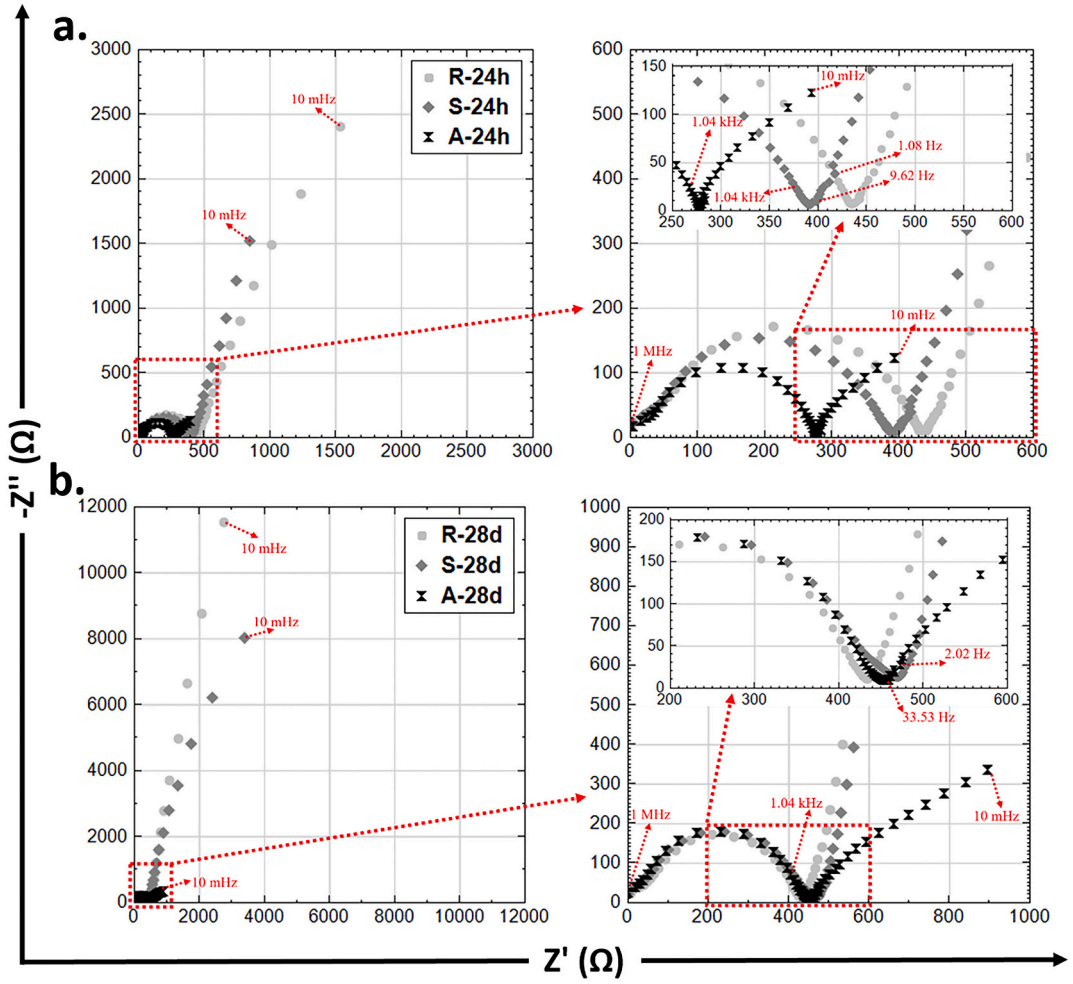

Fig. 14. EIS responses in Nyquist format of specimens treated in water: (a) 24 h-cured; (b) 28 d-cured.

of all specimens depicts the semi-circle capacitive arcs, attributed to the properties of the mortar bulk matrix [65]. The first time constant (R_1C_1) is related to the properties of the mortar bulk matrix. The matrix resistance R_{bulk} (R_1) values of mortar cover are adopted as indicators for bulk matrix properties. The higher resistance of cement-based matrix R_{bulk} (R_1) partly reflects a denser matrix, a lower permeability, and consequently higher strength. The C_{bulk} of mortar/concrete solid phase is in the order of nF [66], and is normally detected in the high frequency range (i.e., approx. 50 kHz to MHz).

3.4.2. *EIS response of Cl-free specimens*

Evidently R-24 h and R-28 d have similar HF EIS response (Fig. 14), which is well in line with the almost identical bond strength of R-24 h and R-28 d (see Fig. 7). Additionally, the higher corrosion resistance of R-28 d compared to R-24 h is reflected by the LF EIS response, and completely in line with the higher R_p from LPR and lower anodic currents from PDP of R-28 d. The higher corrosion resistance of R-28 d leads to a higher bond strength, compared to R-24 h, as illustrated in Fig. 7.

The bond strength at the interface between a steel bar and concrete (mortar) is affected by the corrosion of the steel bar. Corrosion products can alter the steel-mortar interface and influence the development of bond stresses. Research on bond degradation due to reinforcement corrosion has produced a variety of results. Although the results show remarkable scatter, they indicate that the bond strength decreases with the increase of steel corrosion [17].

This, however, is not always a straightforward scenario. For the EIS response of S-24 h and S-28 d, the lower corrosion resistance of S-24 h can be reflected by LF EIS response (lower R_p of S-24 h, as shown in Fig. 18). This is in accordance with the lower anodic current density of S-28 d recorded by PDP. However, a higher bond strength is recorded for S-24 h compared to S-28 d. This is attributed to the altered corrosion product layer (a product layer of different composition and/or distribution) formed on steel surface of S-24 h, together with an obviously different microstructural property at the steel-mortar interface, where initially positive effects of the stray current on cement hydration could have been relevant.

The stray current effect in S-24 h obviously leads to alterations of both product layer (on steel surface) and matrix. The significant accumulation of a product layer in the case of S-24 h is reflected by the PDP response (the plateau region after E_{corr}). Compared to S-28 d, an intermediate (MF to LF) additional time constant is recorded for S-24 h (as marked in inlet of Fig. 14a, in the frequency range of 9.62–1.08 Hz). This is linked to the anodic peaks in the PDP of S-24 h, indicating again the altered steel-mortar interface in the sense of a well adhering product layer on the steel surface (evident from the several anodic current limitations in the PDP response). A lower bulk matrix resistance at the stage of 490 days for S-24 h is reflected by the HF EIS, compared to S-28 d. This implies a more porous bulk and steel-mortar interface of S-24 h, facilitating corrosion products penetration into the bulk matrix, and possibly a more uniform distribution of corrosion products. The consequences of all above are alterations towards a more uniform stress distribution in the system, including the steel-mortar interface and higher bond strength of S-24 h.

For A-24 h and A-28 d, as already shown in the above sections, a

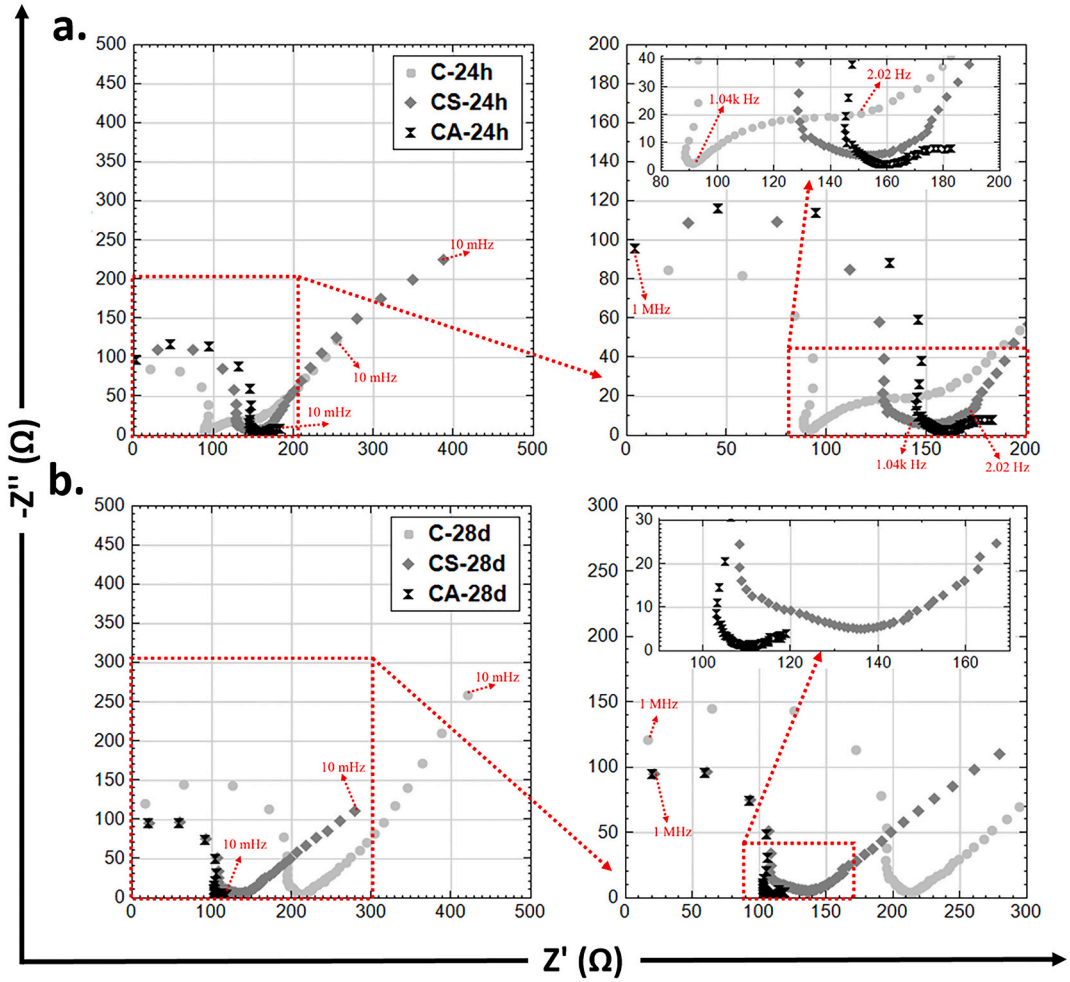

Fig. 15. EIS responses in Nyquist format of specimens treated in 5% NaCl: (a) 24 h-cured; (b) 28 d-cured.

similar global corrosion resistance is recorded by LPR and PDP. However, a bond increase is recorded for A-28 d, while a bond reduction is recorded for A-24 h (Fig. 7). These different bond properties are related to the properties of the mortar matrix, the steel-mortar interface and the product layer. It is clear that the similar shape of the HF semicircle of EIS (a similar semi-circle capacitive arc for the HF time constant) is recorded for both A-24 h and A-28 d (Fig. 14), where 150 Ω higher R_{bulk} for A-28 d is recorded (see Fig. 17), which is normal in view of the more mature A-28 d mortar matrix, compared to A-24 h. This again implies a less porous bulk matrix around the steel surface of A-28 d (compared to A-24 h), and hence a good confinement of the interface (because the corrosion product cannot penetrate into mortar bulk easily). This leads to a higher interaction force between steel surface and mortar cover. The consequence of this is the higher normal stress at steel-mortar interface [67].

This is in line with the anodic limitation of PDP response, as discussed in Section 3.3.1. This can also be reflected by EIS response: an intermediate MF to LF response (in the range of 35.53–2.02 Hz) is recorded for A-28 d. This, together with the two anodic peaks of PDP response of A-28 d, reflect the mixed charge transfer and diffusion processes, which is also indicated by the depressed semi-circular EIS response in the LF (see Fig. 14b). Diffusion accounts for mass transport within the product layer on the steel surface, i.e., it is a proof for a layer that limits anodic dissolution with external polarization, as actually recorded by PDP of A-28 d.

However for A-24 h, the well expressed intermediate time constant is not recorded. On the contrary, an overlap of two constants into a second semi-circular response is observed, which is related to (although limited) charge transfer mainly, i.e., dissolution of corrosion product on the steel surface. This is well supported by anodic dissolution in PDP response (Fig. 13a). This is also in line with the lower R_p derived from EIS (compare with A-28 d), which implies the pronounced corroding status and a thick, porous and non-homogeneous corrosion product layer in A-24 h. The consequence of the above property, is the corresponding reduction of bond strength for A-24 h. It can be summarized that a more porous and volume expanding hydroxide layer will form in conditions of “more water present” in the system (as in A-24). A more open bulk matrix would also result in conditions for corrosion products dissolution and precipitation. In contrast, for A-28 d, Fe oxides-based and/or Ca-substitutes are formed on steel surface (a less porous and volume expanding layer). This together with the mature matrix in A-28 d leads to a confinement of the corrosion products, and maintains structural property at the steel-mortar interface over the duration of these tests.

3.4.3. *EIS response of Cl-containing specimens*

For EIS of specimens C-24 h and CS-24 h (Fig. 15a), a higher corrosion status is relevant for specimen C-24 h (LF EIS response of C-24 h denotes for a more active state of C-24 h, compared to CS-24 h). This conforms to previous results from PDP. This is due to the more significant formation of non-protective and non-adherent corrosion product layer on the steel surface of C-24 h. This again indicates the possible positive effect of stray current on steel surface properties, at early age for CS-24 h, as also discussed. However, the bond strength of C-24 h is higher than that of CS-24 h, irrespective of the lower bulk matrix

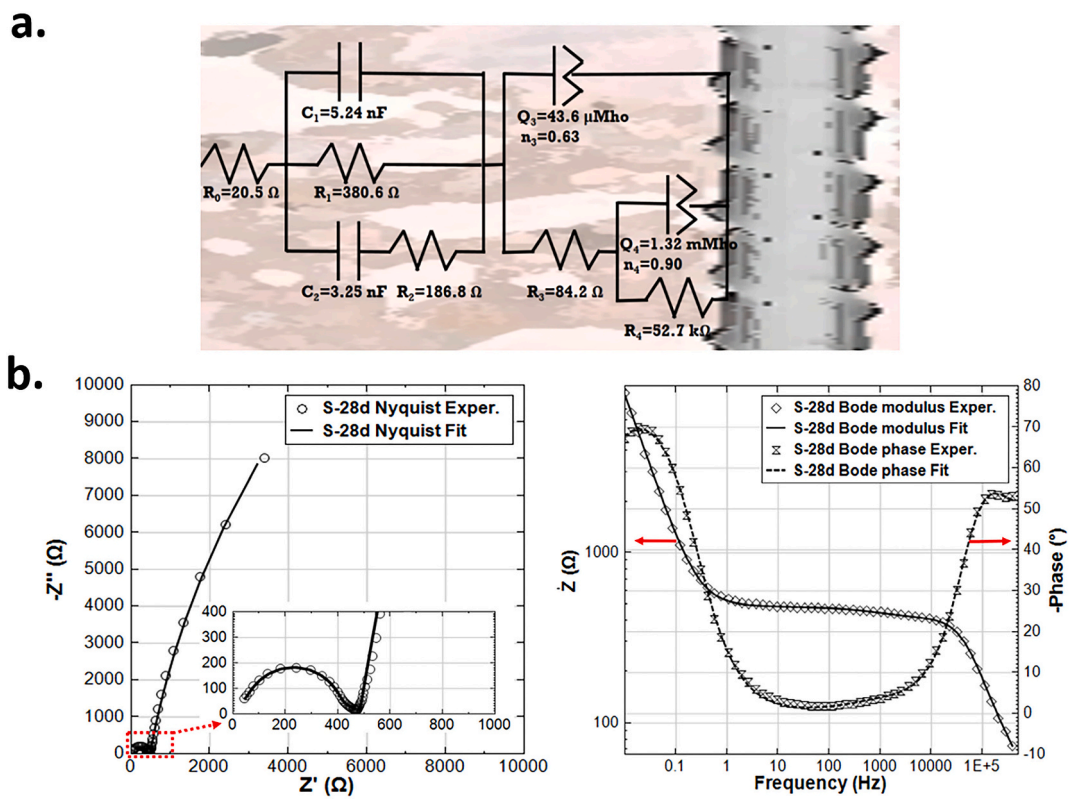

Fig. 16. (a) Equivalent electrical circuit used for fitting, and the best-fit parameters derived on basis of the experimental EIS response of S-28 d at age of 490 days; (b) EIS experimental response (symbols) and fit (lines) of S-28 d at age of 490 days.

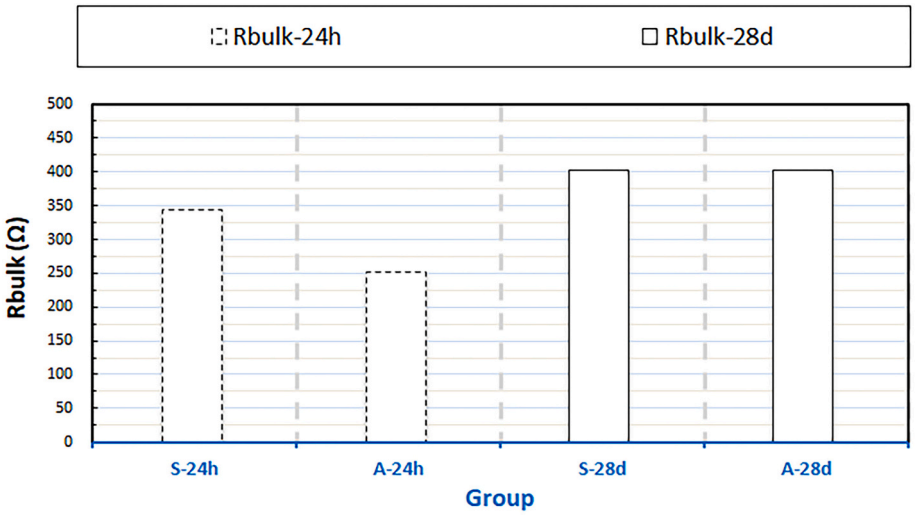

Fig. 17. R_{bulk} values calculated from EIS.

resistance for C-24 h, compared to CS-24 h (Fig. 15a).

Obviously, different properties of the bulk matrix at the steel-mortar interface are relevant for C-24 h, where an additional and very well pronounced time constant can be observed (in the range of 1.04 kHz–2.02 Hz, as marked in Fig. 15a). This is in line with the PDP response of C-24 h, where a limitation after E_{corr} is recorded (Fig. 13b). For C-24 h both EIS and PDP results indicate a larger contribution of a mass transfer control process on the steel surface (evident by the anodic current limitation immediately after E_{corr} in the PDP response and the LF EIS response) and at the steel-mortar interface (evident by the HF EIS response). The limitations are linked to a thick and non-uniform, non-adhering product layer on the steel surface of C-24 h. In contrast, well pronounced additional time constant (HF in EIS response) and anodic limitation after E_{corr} (of PDP) are not observed for CS-24 h. For CS-24 h, though the stray current at early age had positive effect on accelerating cement hydration, stray current also induces mortar softening by substantially increasing the solubility of the C-S-H and CH [1,68–75]. The result will be a coarser pore network structure at the steel-mortar interface, which consequently leads to a decrease of bond strength.

Comparing C-28 d and CS-28 d (Fig. 15b), a lower bond strength is again recorded for the stray current case (CS-28 d). This is in line with the more corrosion resistance of C-28 d, compared to CS-28 d, which is

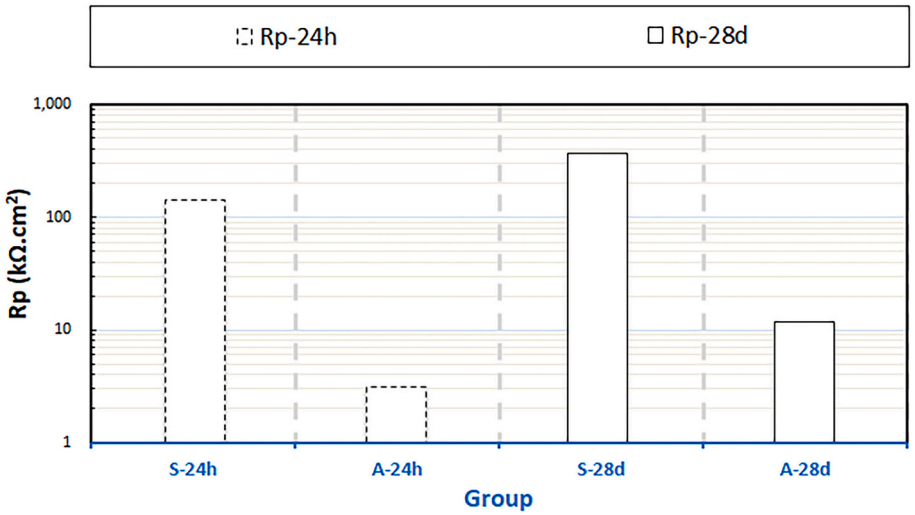

Fig. 18. R_p values calculated from EIS of selected specimens, at 490 days.

also evidenced by both PDP and EIS. In this situation, the stray current adds-up to the "negative" effect of Cl^- and enhances corrosion. It means that for hardened mortar/concrete in aggressive medium, stray current can only enhance damage, rather than exert possible positive effects. This again indicates the importance of the stray current start time (the moment of stray current start).

For CA-24 h and CA-28 d specimens (Cl^- + anodic polarization), a significant bond reduction is recorded. This is in line with the extreme corrosion status confirmed by electrochemical tests. Loss of steel cross-section because of severe corrosion is observed, which subsequently destroys the steel-mortar interface. The pull-out failure modes of CA-24 h and CA-28 d are different: yielding/rupture of steel for CA-24 h, but a complete pull-out of the rebar for CA-28 d. On one hand, a more severe corroding state is observed for CA-28 d. On the other hand, the HF |Z| values of CA-24 h are higher than CA-28 d (see Fig. 15), indicating the denser mortar cover of CA-24 h. The consequence is that the bond strength of steel-mortar interface is higher than the tensile strength of the steel for CA-24 h. Thus the steel rebar is broken before the complete loss of bond. However, for CA-28 d the significantly reduced steel cross-section and lower strength of the mortar cover lead to the smooth process of rebar pull-out.

In summary, the correlation between the electrochemical response (corrosion state of the reinforcing steel and the bulk matrix properties) obtained by the electrochemical measurements (PDP and EIS), and bond properties of steel-mortar interface derived from pull-out tests, is found and established. Although limited range of stray current level is investigated in this research, both PDP and EIS provide valuable insights into the bond strength development and/or degradation of the steel-mortar/concrete interface, as affected by stray current or anodic polarization.

3.5. *Summary of mechanisms for stray current inducing bond loss*

Regardless of whether there is corrodent in the external environment (with or without Cl^- in the present work), anodic polarization leads to more pronounced effects on steel-mortar interface than stray current, in views of both bond behavior and electrochemical response. Though the stray current effect is moderate compared to anodic polarization, the pull-out results show that stray current (at level of 0.3 mA/cm^2) still leads to bond degradation of the steel-mortar interface.

First of all, according to the electrochemical tests, it is clear that the stray current induces steel corrosion (lower corrosion resistance) in all conditions investigated in the present work, compared to the control cases. The stray current induced-steel corrosion is one of the reasons for bond reduction of steel-mortar interface. The corrosion of steel is attributed to the anodic polarization induced by stray current (where stray current flows out from steel surface).

Besides, as already discussed, it is reported that hydration products previously occupying the pore space, would dissolve due to electrical current flow. This will result in vacancies, and coarsening of the pore network [46,76]. The transport of sodium and potassium is faster than that for calcium ions [46,77]. In the stray current electrical field, the sodium (Na^+) or potassium ions (K^+) accumulate more easily, and displace the calcium ion (Ca^{2+}), i.e., reacts with the calcium-silicate-hydrate (C-S-H) phase and $Ca(OH)_2$ (CH) previously formed on steel surface. This initiates mortar dissolution by substantially increasing the solubility of the C-S-H and CH, and leads to bond loss of steel-mortar interface.

Finally, according to the electrochemical tests, it can be noted that the corrosion state of S-24 h is more pronounced than S-28 d. This phenomenon has been aforementioned, i.e., the stray current effects on steel-mortar interface are curing dependent, and linked to the ion/water migration and pore structure development. However, if compared Cl-free cases (S-24 h and S-28 d) to CS-24 and CS-28 d (couple of stray current and Cl^-) cases, the corrosion status of S-24 h and S-28 d are much more moderate. The remarkable corrosion and bond loss were both recorded for CS-24 and CS-28 d. In other words, without corrodent in the external environment (with or without Cl^-), the stray current at this level (of 0.3 mA/cm^2) didn't leads to significant corrosion. However in practical engineering, the DC traction railway tunnels and bridges usually encounter more complex environments or conditions. The wet-dry cycles, temperature or humidity variations, carbonization of concrete cover, other erosion factors, etc., may coexist with stray current. The possible coupled effects of these factors and stray current may lead to more severe corrosion/damages, which are worthy to be further investigated in future research.

4. Conclusions

The effects of stray current on the steel-mortar interface are clarified, in views of both electrochemical properties of steel and bond strength of steel-mortar interface. Correlating the electrochemical property and bond behavior, the following conclusions can be drawn:

1. Stray current (at level of 0.3 mA/cm^2) leads to bond degradation of the steel-mortar interface in all cases (specimens cured in fog room for 24 h or 28 d, then conditioned by supplying stray current or anodic polarization in water or 5% NaCl) investigated in this work.

2. The correlation between the electrochemical response (corrosion state of the reinforcing steel), the bulk matrix properties (derived by EIS), and bond properties of steel-mortar interface (derived from pull-out tests), is established.
3. Regardless of whether there is Cl^- in the external environment, anodic polarization leads to more pronounced effects on the steel-mortar interface, compared to stray current. The anodic polarization produces more corrosion product, the subsequent corrosion product expansion leads to two extremes: the evidently increased bond strength because of more significant confinement at steel-mortar interface; and the significantly reduced bond strength due to the cracking or spalling of the cover. The two effects are bulk matrix properties-dependent. This again indicates the difference between stray current and anodic polarization, in view of affecting bond property of steel-mortar interface.

Declaration of competing interest

The authors declared that they have no conflicts of interest to this work:

We declare that we do not have any commercial or associative interest that represents a conflict of interest related to the work submitted.

Acknowledgments

Zhipei Chen would like to express his gratitude for the financial support from the China Scholarship Council (CSC).

References

[1] J.J. Chang, A study of the bond degradation of rebar due to cathodic protection current, Cem. Concr. Res. 32 (2002) 657–663.
[2] C. Fang, K. Lundgren, L. Chen, C. Zhu, Corrosion influence on bond in reinforced concrete, Cem. Concr. Res. 34 (2004) 2159–2167.
[3] H. Yalciner, O. Eren, S. Sensoy, An experimental study on the bond strength between reinforcement bars and concrete as a function of concrete cover, strength and corrosion level, Cem. Concr. Res. 42 (2012) 643–655.
[4] L. Bertolini, M. Carsana, P. Pedeferri, Corrosion behaviour of steel in concrete in the presence of stray current, Corros. Sci. 49 (2007) 1056–1068.
[5] Z. Chen, D.A. Koleva, K. van Breugel, Electrochemical tests in reinforced mortar undergoing stray current-induced corrosion, in: L.E. Rendon Diaz Miron, D. A. Koleva (Eds.), Concrete Durability: Cementitious Materials and Reinforced Concrete Properties, Behavior and Corrosion Resistance, Springer International Publishing, Cham, 2017, pp. 83–108.
[6] Z. Chen, D. Koleva, K. van Breugel, A review on stray current-induced steel corrosion in infrastructure, Corros. Rev. 35 (2017) 397–423.
[7] A. Susanto, D.A. Koleva, O. Copuroglu, K. van Beek, K. van Breugel, Mechanical, Electrical and microstructural properties of cement-based materials in conditions of stray current flow, J. Adv. Concrete Technol., 11 (2013) 119–134.
[8] A. Aghajani, M. Urgen, L. Bertolini, Effects of DC stray current on concrete permeability, J. Mater. Civ. Eng. 28 (2016).
[9] H. Chu, T. Wang, M.Z. Guo, Z. Zhu, L. Jiang, C. Pan, T. Liu, Effect of stray current on stability of bound chlorides in chloride and sulfate coexistence environment, Constr. Build. Mater. 194 (2019) 247–256.
[10] C. Pan, J. Geng, Q. Ding, Stray current affects the release of bound chloride ions in hydrated cement paste, Int. J. Electrochem. Sci. 13 (2018) 6098–6111.
[11] B. Wang, G.J.J.o.T. Li, Evaluation, the deterioration of cement mortar under the coupled conditions of stray current and sulfate, J. Test. Eval. 49 (2019), JTE20180721.
[12] Y.H. Zhu, Y.S. Zou, J. Geng, F.Z. Wang, Influence of stray current on chloride ion migrates in concrete, J. Wuhan Univ. Technol. 34 (2012) 32–36.
[13] R. Radeka, D. Zorovic, D. Barisin, Influence of frequency of alternating current on corrosion of steel in seawater, Anti-Corros. Methods Mater. 27 (1980), 13-15+19.
[14] V. Kolar, R. Hrbac, Measurement of ground currents leaking from DC electric traction, electric power engineering (EPE), in: Proccedings of the 2014 15th International Scientific Conference on, IEEE, 2014, pp. 613–617.
[15] M. Ormellese, S. Goidanich, L. Lazzari, M. Pedeferri, F. Bolzoni, Laboratory testing on the influence of alternated current on steel corrosion, in: Corrosion 2004, NACE International, New Orleans, Louisiana, 2004, p. 11.
[16] G. Malumbela, M. Alexander, P. Moyo, Interaction between corrosion crack width and steel loss in RC beams corroded under load, Cem. Concr. Res. 40 (2010) 1419–1428.
[17] Y. Zhao, H. Lin, K. Wu, W. Jin, Bond behaviour of normal/recycled concrete and corroded steel bars, Constr. Build. Mater. 48 (2013) 348–359.
[18] C. Lingvay, A. Cojocaru, T. Vişan, I. Lingvay, Degradations of reinforced concrete structures due to d.c. and a.c. stray currents, UPB Scientific Bulletin, Series B: Chemistry and Materials Science 73 (2011) 143–152.
[19] H.W. Teng, S.M. Yang, Z.C. Shu, Y. Huang, D. Huo, Simulation experiment of loading influence to reinforcement corrosion affected by stray current and salt solution, J. Wuhan Univ. Technol. 32 (2010) 147–151.
[20] Z.J. Dong, X.Y. Li, P. Yan, F. Xing, Distribution of the stray current of rebar in the ballast bed, Appl. Mech. Mater. (2012) 2147–2153.
[21] Y. Luo, C. Wang, C. Luo, Q. Huang, S. Wang, X. Peng, Effect of electrical field on TSA failure of cement-based materials, Cem. Concr. Res. 90 (2016) 19–26.
[22] A. Brenna, L. Lazzari, M. Ormellese, Stray current control by a new approach based on current monitoring on a potential probe, Corros. Eng. Sci. Technol. 52 (2017) 359–364.
[23] K. Tang, Stray current induced corrosion of steel fibre reinforced concrete, Cem. Concr. Res. 100 (2017) 445–456.
[24] J. Tinnea, R. Tinnea, D. Burke, L. Nelson, S. Cochran, E. Anderson, L. Pham, Evaluating Concrete Resistivity: Reducing Stray Current from dc Streetcars, NACE International.
[25] M. Narozny, K. Zakowski, K. Darowicki, Method of sacrificial anode dual transistor-driving in stray current field, Corros. Sci. 98 (2015) 605–609.
[26] C. Wang, W. Li, Y. Wang, S. Xu, X. Yang, Chloride-induced stray current corrosion of Q235A steel and prediction model, Constr. Build. Mater. 219 (2019) 164–175.
[27] M. Chen, K. Wang, Q. Wu, Z. Qin, An experimental corrosion investigation of coupling chloride ions with stray current for reinforced concrete, Appl. Mech. Mater. 166–169 (2012) 1987–1993.
[28] K. Wang, Q.S. Wu, M.C. Chen, L. Xie, Corrosion fatigue of reinforced concrete in the presence of stray current, in: 2011 International Conference on Electric Technology and Civil Engineering, ICETCE 2011 Lushan, 2011, pp. 1133–1136.
[29] X. Wang, X. Song, Y. Chen, Z. Wang, L. Zhang, Study on corrosion and delamination behavior of X70 steel under the coupling action of AC-DC interference and stress, Int. J. Electrochem. Sci. 14 (2019) 1968–1985.
[30] C. Wen, J. Li, S. Wang, Y. Yang, Experimental study on stray current corrosion of coated pipeline steel, J. Nat. Gas Sci. Eng. 27 (2015) 1555–1561.
[31] F.E. Sloan, J.B. Talbot, Corrosion of graphite-fiber-reinforced composites IIAnodic polarization damage, Corros. 48 (1992) 7.
[32] C. Wang, W. Li, G. Xin, Y. Wang, S. Xu, Prediction model of corrosion current density induced by stray current based on QPSO-driven neural network, Complexity 2019 (2019), 3429816.
[33] G. Cui, Z.L. Li, C. Yang, M. Wang, The influence of DC stray current on pipeline corrosion, Pet. Sci. 13 (2016) 135–145.
[34] A.O.S. Solgaard, M. Carsana, M.R. Geiker, A. Küter, L. Bertolini, Experimental observations of stray current effects on steel fibres embedded in mortar, Corros. Sci. 74 (2013) 1–12.
[35] G. Xu, H.F. Fei, Y.M. Wang, Q. Wang, Research on corrosion characteristics of stainless steel bar in stray current and chloride ion coexisted environment, Adv. Mater. Res. 261–263 (2011) 56–60.
[36] Q.J. Zhu, A.L. Cao, Z.F. Wang, J.W. Song, S.L. Chen, Fundamental aspects of stray current corrosion on buried pipeline, Adv. Mater. Res. 146–147 (2010) 70–74.
[37] Z. Chen, D. Koleva, Corrosion behavior of reinforcing steel undergoing stray current and anodic polarization, Materials 14 (2021) 261.
[38] Standard practice for preparing, cleaning, and evaluating corrosion test specimens, in: Annual Book of ASTM Standards, 2003, pp. 17–25.
[39] C. Wu, G. Chen, J.S. Volz, R.K. Brow, M.L. Koenigstein, Local bond strength of vitreous enamel coated rebar to concrete, Constr. Build. Mater. 35 (2012) 428–439.
[40] L. Chung, J.-H. Jay Kim, S.-T. Yi, Bond strength prediction for reinforced concrete members with highly corroded reinforcing bars, Cem. Concr. Compos. 30 (2008) 603–611.
[41] A. Torre-Casanova, L. Jason, L. Davenne, X. Pinelli, Confinement effects on the steel-concrete bond strength and pull-out failure, Eng. Fract. Mech. 97 (2012) 92–104.
[42] M. Stern, A.L. Geary, Electrochemical polarization: I. a theoretical analysis of the shape of polarization curves, J. Electrochem. Soc. 104 (1957) 56–63.
[43] J.A. Gonzalez, S. Algaba, C. Andrade, Corrosion: of reinforcing bars in carbonated concrete, Br. Corros. J. 15 (1980) 135–139.
[44] C. Andrade, J.A. González, Quantitative measurements of corrosion rate of reinforcing steels embedded in concrete using polarization resistance measurements, Mater. Corros. 29 (1978) 515–519.
[45] Standard test method for comparing concrete on the basis of the bond developed with reinforcing steel, ASTM annual book of standards: Section 4. Construction, (1991).
[46] A. Susanto, D.A. Koleva, K. Van Breugel, K. Van Beek, Stray current-induced development of cement-based microstructure in water-submerged, Ca(OH)2-submerged and sealed conditions, J. Adv. Concr. Technol. 15 (2017) 244–268.
[47] A. Susanto, D.A. Koleva, K. Van Breugel, The effect of water-to-cement ratio and curing on material properties of mortar specimens in stray current conditions, J. Adv. Concr. Technol. 15 (2017) 627–643.
[48] M. Čekerevac, M. Simičić, L.N. Bujanović, N. Popović, The influence of silicate and sulphate anions on the anodic corrosion and the transpassivity of iron and silicon-rich steel in concentrated KOH solution, Corros. Sci. 64 (2012) 204–212.
[49] S.T. Amaral, I.L. Müller, A RRDE study of the electrochemical behavior of iron in solutions containing silicate and sulphate at pH 10-13, Corros. Sci. 41 (1999) 759–771.
[50] G.T. Burstein, G.W. Askley, Early steps in the anodic oxidation of iron in aqueous solution, Corros. 39 (1983) 241–247.
[51] A. Fattah-alhosseini, A. Saatchi, M.A. Golozar, K. Raeissi, The transpassive dissolution mechanism of 316L stainless steel, Electrochim. Acta 54 (2009) 3645–3650.

[52] D.A. Koleva, N. Boshkov, K. van Breugel, J.H.W. de Wit, Steel corrosion resistance in model solutions, containing waste materials, Electrochim. Acta 58 (2011) 628–646.
[53] A. Covelo, B. Díaz, L. Freire, X.R. Nóvoa, M.C. Pérez, Microstructural changes in a cementitious membrane due to the application of a DC electric field, J. Environ. Sci. Health, Part A: Environ. Sci. Eng. Toxic Hazard. Subst. Control 43 (2008) 985–993.
[54] B. Díaz, L. Freire, P. Merino, X.R. Nóvoa, M.C. Pérez, Impedance spectroscopy study of saturated mortar samples, Electrochim. Acta 53 (2008) 7549–7555.
[55] G. Song, Equivalent circuit model for AC electrochemical impedance spectroscopy of concrete, Cem. Concr. Res. 30 (2000) 1723–1730.
[56] O. Poupard, A. Aït-Mokhtar, P. Dumargue, Corrosion by chlorides in reinforced concrete: determination of chloride concentration threshold by impedance spectroscopy, Cem. Concr. Res. 34 (2004) 991–1000.
[57] M.F. Montemor, M.P. Cunha, M.G. Ferreira, A.M. Simões, Corrosion behaviour of rebars in fly ash mortar exposed to carbon dioxide and chlorides, Cem. Concr. Compos. 24 (2002) 45–53.
[58] V. Feliu, J.A. González, C. Andrade, S. Feliu, Equivalent circuit for modelling the steel-concrete interface. I. Experimental evidence and theoretical predictions, Corros. Sci. 40 (1998) 975–993.
[59] C. Andrade, L. Soler, C. Alonso, X.R. Nóvoa, M. Keddam, The importance of geometrical considerations in the measurement of steel corrosion in concrete by means of AC impedance, Corros. Sci. 37 (1995) 2013–2023.
[60] F. Wenger, J. Galland, Analysis of local corrosion of large metallic structures or reinforced concrete structures by electrochemical impedance spectroscopy (EIS), Electrochim. Acta 35 (1990) 1573–1578.
[61] V. Feliu, J.A. González, S. Feliu, Algorithm for extracting corrosion parameters from the response of the steel-concrete system to a current pulse, J. Electrochem. Soc. 151 (2004) B134–B140.
[62] D.A. Koleva, A.G. Denkova, N. Boshkov, K. Van Breugel, Electrochemical performance of steel in cement extract and bulk matrix properties of cement paste in the presence of Pluronic 123 micelles, J. Mater. Sci. 48 (2013) 2490–2503.
[63] A.A. Sagüés, S.C. Kranc, E.I. Moreno, The time-domain response of a corroding system with constant phase angle interfacial component: application to steel in concrete, Corros. Sci. 37 (1995) 1097–1113.
[64] A.A. Sagüés, M.A. Pech-Canul, A.K.M. Shahid Al-Mansur, Corrosion macrocell behavior of reinforcing steel in partially submerged concrete columns, Corros. Sci. 45 (2003) 7–32.
[65] A. Blagojevic, D.A. Koleva, J.C. Walraven, Monitoring Steel Corrosion in Reinforced Concrete Beams with Variable Crack Widths under Sustained Load, EUROCORR 2014, European Corrosion Congress, Pisa, Italy, 2014, 8–12 September 2014.
[66] C. Andrade, L. Soler, X.R. Nóvoa, Advances in electrochemical impedance measurements in reinforced concrete, Mater. Sci. Forum 192–194 (1995) 843–856.
[67] A.A. Almusallam, A.S. Al-Gahtani, A.R. Aziz, Rasheeduzzafar, Effect of reinforcement corrosion on bond strength, Constr. Build. Mater., 10 (1996) 123–129.
[68] J. García, F. Almeraya, C. Barrios, C. Gaona, R. Núñez, I. López, M. Rodríguez, A. Martínez-Villafañe, J.M. Bastidas, Effect of cathodic protection on steel–concrete bond strength using ion migration measurements, Cem. Concr. Compos. 34 (2012) 242–247.
[69] E. Garcia-Diaz, J. Riche, D. Bulteel, C. Vernet, Mechanism of damage for the alkali-silica reaction, Cem. Concr. Res. 36 (2006) 395–400.
[70] M.B. Haha, E. Gallucci, A. Guidoum, K.L. Scrivener, Relation of expansion due to alkali silica reaction to the degree of reaction measured by SEM image analysis, Cem. Concr. Res. 37 (2007) 1206–1214.
[71] A. Leemann, B. Lothenbach, The influence of potassium-sodium ratio in cement on concrete expansion due to alkali-aggregate reaction, Cem. Concr. Res. 38 (2008) 1162–1168.
[72] R. Narayan Swamy, M.M. Al-Asali, Expansion of concrete due to alkali-silica reaction, ACI Mater. J. 85 (1988) 33–40.
[73] J.M. Ponce, O.R. Batic, Different manifestations of the alkali-silica reaction in concrete according to the reaction kinetics of the reactive aggregate, Cem. Concr. Res. 36 (2006) 1148–1156.
[74] Y. Hong, Z. Li, G. Qiao, J. Ou, Numerical simulation and experimental investigation of the stray current corrosion of viaducts in the high-speed rail transit system, Constr. Build. Mater. 157 (2017) 416–423.
[75] K. Ishii, H. Seki, T. Fukute, K. Ikawa, Cathodic protection for prestressed concrete structures, Constr. Build. Mater. 12 (1998) 125–132.
[76] M. Castellote, C. Andrade, M.C. Alonso, Changes in concrete pore size distribution due to electrochemical chloride migration trials, ACI Mater. J. 96 (1999) 314–319.
[77] H. Saito, S. Nakane, S. Ikari, A. Fujiwara, Preliminary experimental study on the deterioration of cementitious materials by an acceleration method, Nucl. Eng. Des. 138 (1992) 151–155.